Published in final edited form as:
J Neurosci. 2009 September 9; 29(36): 11123–11133. doi:10.1523/JNEUROSCI.2232-09.2009.

Atoh1-lineal neurons are required for hearing and for the survival of neurons in the spiral ganglion and brainstem accessory auditory nuclei

Stephen M. Maricich, **Anping Xia**, **Erin L. Mathes**, **Vincent Y. Wang**, **John S. Oghalai**, **Bernd Fritzsch**, and **Huda Y. Zoghbi**

Abstract

Atoh1 is a basic helix-loop-helix transcription factor necessary for the specification of inner ear hair cells and central auditory system neurons derived from the rhombic lip. We used the *Cre-loxP* system and two *Cre*-driver lines ($Egr2^{Cre}$ and $Hoxb1^{Cre}$) to delete *Atoh1* from different regions of the cochlear nucleus (CN) and accessory auditory nuclei (AAN). Adult *Atoh1*-conditional knockout mice ($Atoh1^{CKO}$) are behaviorally deaf, have diminished auditory brainstem evoked responses and disrupted CN and AAN morphology and connectivity. In addition, *Egr2;* $Atoh1^{CKO}$ mice lose spiral ganglion neurons in the cochlea and AAN neurons during the first 3 days of life, revealing a novel critical period in the development of these neurons. These new mouse models of predominantly central deafness illuminate the importance of the CN for support of a subset of peripheral and central auditory neurons.

INTRODUCTION

Deafness is one of the most common sensory abnormalities in humans, affecting an estimated 16.1% (29 million people) of the US population (Agrawal et al., 2008). The pathology leading to deafness can occur in the peripheral and/or central nervous system. Peripheral hearing impairment comprises the majority of cases and arises from gross cochlear malformations; dysfunction of cochlear hair cells, which detect auditory stimuli and transmit the signal to spiral ganglion neurons (SGNs); dysfunction of the constant ionic current flow within the cochlea necessary for normal hair cell transduction; and/or dysfunction of the auditory nerve, which contains SGN axons and relays the auditory signal to the brainstem cochlear nucleus (CN). Central hearing impairment arises from disruption of the central auditory pathways, which are comprised of two parts. The main pathway for sound perception runs from the CN through the lateral lemniscus to the nuclei of the inferior colliculus, which in turn relay auditory information to the medial geniculate bodies of the thalamus and on to the temporal lobes. The other pathway travels from the CN through the trapezoid body to the accessory auditory nuclei (AAN) of the brainstem, which are comprised of the superior olivary complex (SOC) and the nuclei of the trapezoid body (NTB). These nuclei are thought to function in the localization of the temporal and spatial origins of sounds (Willott, 2001). The etiologies of primary central deafness are varied; examples include brainstem malformations, environmental causes (such as fetal alcohol syndrome), dementia, CNS infection, stroke and trauma (Griffiths, 2002). Unfortunately, the pathogenesis of deafness caused by central defects is poorly understood, in part due to the

Corresponding authors: Stephen M. Maricich, Departments of Pediatrics and Neurosciences, Case Western Reserve University School of Medicine, 216-368-2194, smm18 @case.edu, Huda Y. Zoghbi, Department of Neuroscience, Baylor College of Medicine, 713-798-6523, hzoghbi@bcm.edu.

absence of genetic animal models that selectively affect these components of the auditory pathway.

Atoh1, or *Math1*, is a basic helix-loop-helix transcription factor important for the development of cells in the peripheral and central portions of the auditory system. In the peripheral auditory system, *Atoh1* is both necessary and sufficient to direct the differentiation and maintenance of hair cells of the cochlea (Bermingham et al., 1999).

In the central nervous system, *Atoh1* is necessary for the specification of populations of neurons in the nuclei of the dorsal lateral lemniscus and CN, which derive mostly from the *Atoh1*-expressing dorsal region of the developing embryonic hindbrain known as the rhombic lip (Akazawa et al., 1995; Ben-Arie et al., 1996; Wang et al., 2005). We hypothesized that deletion of *Atoh1* exclusively in regions of the developing central nervous system would create an excellent model of central deafness and would provide insight regarding the connectivity and maintenance of the central pathways.

To test our hypothesis, we used knowledge of the spatial embryonic origins of the CN (Marin and Puelles, 1995; Cambronero and Puelles, 2000; Cramer et al., 2000; Farago et al., 2006) to design an experimental paradigm using *Cre-loxP* technology to specifically ablate expression of *Atoh1* in areas of the murine rhombic lip known to contribute neurons to the developing CN. We demonstrate that loss of *Atoh1* expression in these hindbrain regions results in primary loss of neurons from the CN and AAN. This neuronal loss causes secondary disruption of both the peripheral and central auditory systems, possibly due to loss of trophic support for these neuronal populations.

METHODS

Mice and mating paradigms

The generation of $Atoh1^{CreER\text{-}T2}$, $Atoh1^{flox}$, $Atoh1^{LacZ}$, $Egr2^{Cre}$, $Hoxb1^{Cre}$ and $ROSA^{R26R}$ mice were described previously (Ben-Arie et al., 1996; Soriano, 1999; Voiculescu et al., 2000; Arenkiel et al., 2003; Machold and Fishell, 2005; Shroyer et al., 2007). All animals used for these experiments were maintained on mixed genetic backgrounds except for the $Atoh1^{LacZ}$ and $ROSA^{R26R}$ mice, which are congenic on the C57Bl/6J strain background.

Atoh1 conditional knockout ($Atoh1^{CKO}$) mice were generated by first crossing either $Egr2^{Cre}$ mice or $Hoxb1^{Cre}$ mice with $Atoh1^{LacZ}$ mice to generate $Egr2^{Cre/+}$; $Atoh1^{LacZ/+}$ and $Hoxb1^{Cre/+}$; $Atoh1^{LacZ/+}$ double transgenic animals. These animals were mated with $Atoh1^{flox/flox}$ mice to generate triple transgenic mice of four genotypes: $Cre^{+/+}$; $Atoh1^{+/flox}$, $Cre^{Cre/+}$; $Atoh1^{+/flox}$, $Cre^{+/+}$; $Atoh1^{LacZ/flox}$ and $Cre^{Cre/+}$; $Atoh1^{LacZ/flox}$. Only animals with $Egr2^{Cre}$ and $Atoh1^{LacZ}$ or $Hoxb1^{Cre}$ and $Atoh1^{LacZ}$ alleles lack *Atoh1* expression in the $Egr2^{Cre}$ (*Egr2; Atoh1*^{CKO}) or $Hoxb1^{Cre}$ (*Hoxb1; Atoh1*^{CKO}) distributions. Mice of the other three genotypes ($Cre^{+/+}$*; Atoh1*$^{+/flox}$, $Cre^{Cre/+}$*; Atoh1*$^{+/flox}$, and $Cre^{+/+}$*; Atoh1*$^{LacZ/flox}$) are collectively referred to as “wildtype” because they display no abnormal phenotypes and are indistinguishable based on the testing reported here.

Behavioral testing

Acoustic startle responses of 2–10 month-old mice (6–15 mice of each genotype) were measured using the SR-Lab System (San Diego Instruments, San Diego, CA). Mice were placed in a Plexiglas cylinder and left undisturbed for 5 minutes, and 70 dB background white noise was played throughout the testing period. Test sessions consisted of six blocks of eight different trial types presented in pseudorandom order such that each trial type occurred once within a block of eight trials (average inter-trial interval = 15 seconds, range = 10–20 seconds). One trial type consisted of the startle stimulus alone, which was a 120 dB pure tone sound

played for 40 ms. Three different "prepulse" trial types consisted of 20 ms sounds of 74, 78, or 82 dB presented 100 ms before the 120 dB startle stimulus. These three prepulse sounds were also presented separately without the startle stimulus. Finally, trials where no stimulus was presented were used to establish the startle baseline. The startle response, consisting of movement by the test mouse when the sounds were played, was recorded every 1 ms for 65 ms starting with the onset of the stimulus trial, and the maximum startle amplitude recorded during the 65-ms sampling window was used for comparison between mice of different genotypes.

Electrophysiological testing

Our methodology for measuring ABR, DPOAE, CAP and CM in mice has been described previously (Xia et al., 2007). Briefly, 6–7 week-old mice were anesthetized using ketamine (100mg/kg) and xylazine (5 mg/kg). Mice were placed on a heating pad to maintain normal body temperature throughout the test procedures. Different sets of animals were used for ABR/DPOAE (n = 6–9 per genotype) and CAP/CM (n = 3 – 4 per genotype) measurements; typical recording times ranged from 25–40 minutes. Acoustic stimuli were generated digitally, converted to analog signals, and then attenuated to the appropriate intensity according to our experimental design (RP2 and PA5, Tucker-Davis Technologies). Two different speaker systems were used: high frequency piezoelectric speakers for the ABR and DPOAE measurements (EC1, Tucker-Davis Technologies) and a supertweeter (Radio Shack) for the CAP and CM measurements. The speakers were connected to an ear bar inserted into the ear canal and calibrated from 4 to 95 kHz by a probe-tip microphone (type 8192, NEXUS conditioning amplifier, Bruel and Kjar, Denmark) inserted through the earbar. The tip of the microphone was within 3 mm of the tympanic membrane.

The ABR was measured from a needle electrode positioned at the ventral surface of the tympanic bulla referenced to an electrode placed at the vertex of the skull. A ground electrode was placed in the hind leg. The stimulus was a 5 ms sine wave tone pip of alternating polarity with cos2 envelope rise and fall times of 0.5 ms and a repetition time of 50 ms. The stimulus intensity ranged from 10 to 80 dB SPL in 10 dB steps. The frequency range studied was 4 to 90 kHz. Two hundred fifty ABR responses were sampled at each frequency over the 50 ms repetition time and averaged. Thresholds were calculated by interpolating the peak-to-peak voltages of the ABR waveforms over the range of stimulus intensities and determining when the ABR was four standard deviations above the noise floor. If no ABR response was detected at our equipment limit of 80 dB SPL, we arbitrarily defined the threshold to be 80 dB.

To measure the CAP, a surgical procedure was performed to open the tympanic bulla. The anesthetized mouse was secured rigidly in a head holder, a ventral incision was made, and the pinna was resected. The bulla was carefully opened medial to the tympanic annulus and the earbar was secured within the ear canal. The CAP was measured from the ball-ended tip of a Teflon-coated silver wire (0.003 inch diameter, AM Systems, Carlsborg, WA) advanced onto the round window membrane with a micromanipulator. The signal was referenced to a silver wire inserted under the skin near the vertex of the skull. The ground electrode was placed in the hind leg. The stimulus used to elicit the CAP was identical to that used to elicit the ABR, however only 24 repetitions were averaged at each stimulus intensity level.

The stimuli for eliciting DPOAEs were two sine wave tones of differing frequencies (F2 = 1.2*F1) of 1 second duration with F2 ranging from 4 to 90 kHz. The two tones were presented at identical intensities, which ranged from 20–80 dB SPL in 10 dB increments. The acoustic signal picked up by the microphone in the earbar was digitized at 200 kHz and the magnitude of the 2*F1-F2 distortion product determined by fast Fourier transform (FFT). The surrounding noise floor was also calculated by averaging 20 adjacent frequency bins around the distortion product frequency. DPOAE thresholds were calculated off-line by interpolating the data and

identifying when the signal was > −5 dB SPL and greater than two standard deviations above the noise floor. If no DPOAE response was detected at our equipment limits of 80 dB SPL, we arbitrarily defined the threshold to be 80 dB.

The CM signal was measured from a silver wire placed on the round window membrane, as described for the CAP measurement. The stimulus was a 30 ms 6 kHz tone repeated every 1 second, and its intensity was ranged from 10–100 dB SPL. By measuring the speaker output with the probe tip microphone in the ear bar, FFT analysis demonstrated that all stimulus harmonics and noise at all other frequencies were at least 50 dB below the primary signal at all stimulus intensities. The CM signal measured by the bioamplifier was digitized at 200 kHz and the magnitude of the response at 6 kHz determined by FFT.

Tissue harvesting and processing

For embryonic tissue, pregnant dams were euthanized and embryos dissected into cold 1X PBS. Either whole embryos (E9.5) or dissected heads and brains (E16-P0) were immersion-fixed for 30 minutes-overnight at 4°C in either fresh 4% paraformaldehyde (PFA)/0.1M phosphate buffer or 10% neutral buffered formalin (NBF; Fisher). Mice 3 days of age and older were transcardially perfused with 10% NBF. Brains and heads were dissected at P3, while for older ages brains and cochlea were dissected and tissues were post-fixed overnight at 4°C. Following fixation, all tissues were washed three times in 1X PBS. Brains were stored in 70% EtOH for paraffin embedding or 30% sucrose/1X PBS for cryoembedding. Heads and cochlea were decalcified in 0.12M EDTA for 5 days, then transferred to 70% EtOH and embedded in paraffin.

For lipophilic dye injections, P0-P18 mice were anesthetized with 60 mM tribromoethanol (Avertin) and then transcardially perfused with cold 1X PBS followed by cold 4% PFA/0.1M phosphate buffer. Heads were stored in 0.4% PFA/0.1M PB at 4°C until the time of dye injection.

For paraffin sectioning, tissues were dehydrated and embedded in Paraplast (McCormick Scientific) or TissuePrep (Fisher). Six μm serial sections were cut on a Leica microtome and collected on Superfrost®/Plus slides (Fisher).

For cryostat sectioning, tissues were embedded in Tissue-Tek OCT (Sakura Finetek), serially-sectioned at 20–25 μm on a freezing microtome, and collected on Superfrost®/Plus slides.

Histology

Embryonic and P0 tissues were stained for β-galactosidase activity in wholemount preparations for 2–24 hours at 37° C. Tissues were then washed three times in 1X PBS and transferred to 70% EtOH for storage. Slides with cryostat sections of adult brain were stained in a similar fashion, then counterstained with Nuclear Fast Red (Vector Labs), dehydrated, and mounted with Cytoseal 60 (Richard-Allan Scientific).

Paraffin sections from brains of all ages were rehydrated and stained with Cresyl Violet, then dehydrated and coverslipped. Paraffin sections of heads and cochlea of all ages were rehydrated and sequentially stained with Mayer's Hematoxylin and Eosin Y (Sigma), followed by dehydration and coverslipping.

For all histological analyses (Cresyl Violet, X-gal, immunochemistry and *in situ* hybridization), series of slides were processed to allow exact matching of the anteroposterior levels between wildtype, *Egr2; Atoh1*^{CKO} and *Hoxb1; Atoh1*^{CKO} brains.

Immunochemistry

Tissue sections from at least two brains of each genotype were blocked for 1–2 hours at room temperature (RT) in 1X PBS/0.3% Triton X-100 (PBST) with 2% normal goat or donkey serum (PBST-S). Slides were incubated at 4°C overnight in primary antibodies diluted in PBST-S: mouse anti-Cat-301 (MAB5284, Millipore) 1:500; chicken anti-choline acetyltransferase (AB15468, Chemicon) 1:2000. Goat anti-mouse (Jackson Immunoresearch) and donkey anti-goat (Jackson Immunoresearch) secondary antibodies conjugated to Cy3 were used at a 1:500 dilution in PBST-S and applied for 30 minutes at RT. For horseradish peroxidase staining (ChAT), HRP-conjugated goat anti-chicken secondary antibody from Vector Labs was used following manufacturer's directions.

Goat polyclonal anti-RORα (SC-6062, Santa Cruz Biotechnology) was used on antigen retrieved tissue (Ino, 2004). Following fixation and prior to cryoembedding, brains were cut into 3–5 mm thick slices in the coronal plane and boiled for 3 minutes in 10 mM sodium citrate buffer, pH 6.0. A 1:2000 dilution of the primary antibody was used in PBST in 2% normal donkey serum. Diaminobenzidine labeling was performed using a Vectastain kit (Vector Labs) according to manufacturer's instructions.

In situ hybridization

Tissue preparation and automated ISH were performed as previously described (Carson et al., 2002; Visel et al., 2004; Yaylaoglu et al., 2005) and as described online at http://www.genepaint.org/RNA.htm. Briefly, heads of embryonic mice were embedded in OCT and fresh frozen in a custom-made freezing chamber that allows stereotaxic alignment of the specimen. Serial sections were cut at 20 μm thickness on a freezing microtome. After PFA fixation and acetylation the slides were assembled into flow-through hybridization chambers and placed into a Tecan (Mannedorf, Switzerland) Genesis 200 liquid-handling robot, which executes a script that performs non-radioactive ISH in less than 24 hrs. Antisense probes for *Atoh1* and *VGLUT2* were generated from PCR-amplified cDNA clones and used for *in vitro* transcription of digoxygenin-labeled riboprobe using either T7 or SP6 RNA polymerase. Robotic ISH was performed according to a previously published protocol (Yaylaoglu et al., 2005). Hybridized antisense probe was detected by catalyzed reporter deposition (CARD) using biotinylated tyramide followed by colorimetric detection of biotin with avidin coupled to alkaline phosphatase (Carson et al., 2005; Yaylaoglu et al., 2005). At least two brains of each genotype were analyzed.

Atoh1-lineal fate mapping

Pregnant dams obtained from matings of $Atoh1^{CreER\text{-}T2}$ and $ROSA^{R26R}$ animals were intraperitoneally injected at E9.5 or E10.5 with 4mg (200 μL) of a 20mg/mL solution of tamoxifen (Sigma) dissolved in corn oil. Embryos were harvested on day E18.5 of gestation.

Lipophilic dye injections

Wedges soaked with lipophilic dyes of different colors (Fritzsch et al., 2005) were injected into the ear (base, apex and vestibular organs) or the brainstem (ventral acoustic stria, cochlear nuclei) using appropriate landmarks (trigeminal nerve or facial nerve) of P0–P19 conditional knockout and wildtype mice. Brains and ears were incubated for 7–14 days (depending on age) at 36°C in 4% PFA. Ears were dissected and imaged as whole mounts to ensure application accuracy. Brains were viewed as whole mounts and subsequently embedded in 4% gelatin and hardened for 10 days in 10% PFA at 4°C. One hundred μm thick coronal sections were mounted in glycerol and viewed with a Zeiss LSM 510 or Leica SPE confocal microscope using appropriate filter settings. Image stacks along the Z-axis were taken and combined using Zeiss LSM or Leica software. Two or three brains or cochlea from each genotype were analyzed.

Cell and axon counts

Spiral ganglion neuron (SGN) counts were done on 6 μm paraffin sections. Consecutive sections through the entire spiral ganglion were stained with Mayer's Hematoxylin/Eosin Y, and all SGNs with a clear nuclear membrane were counted on every 5th section (every 30 μm) at 200 × magnification on a Zeiss Axioplan 2 microscope (Zeiss Instruments). Neurons and pyknotic nuclei of the medial nucleus of the trapezoid body (MNTB) were counted in a similar fashion, except every 10th (every 60 μm; P0, P3, P7) or every 20th (every 120 μm; adult) section was analyzed. A total of 3 or 4 cochlea and 4 MNTBs from 2 animals of each genotype at each age were counted.

Axonal counts were obtained from three ears of P17–19 wildtype (*Egr2*$^{+/+}$*; Atoh1*$^{LacZ/flox}$) and *Egr2; Atoh1*^{CKO} mice. For this, ears were osmicated and tangential sections were taken parallel to the basal hook region and the middle turn (Postigo et al., 2002). Images were taken from the middle and basal cochlear turns using a Nikon E800 with a 60× oil immersion lens (NA 1.4) and all myelinated axons in a 100 μm stretch of these sections were counted on prints as previously described (Postigo et al., 2002).

To correct for overcounting of SGNs, digital photographs of all regions of the spiral ganglion were taken in a single mid-modiolar section using a Zeiss Axiocam and nuclear diameters were measured using Zeiss Axiovision software (Version 4.5). The Hendry method (Hendry, 1976) was used to correct for over-representation of nuclei in multiple sections. No corrections were done for axon counts.

Statistical analysis

All statistical analysis was done using SPSS version 11 for Mac OS-X (SPSS Inc.). ANOVA was used to compare ABR, acoustic startle, CAP, CM and DPOAE values across genotypes, followed by calculation of least-square differences for pair-wise comparisons. Cell and axon counts were compared using independent sample two-tailed t-tests.

RESULTS

Deletion of *Atoh1* from rhombomeres 3–5 disrupts cochlear nucleus formation

The *Egr2*^{Cre} line drives *Cre* expression specifically in rhombomeres 3 and 5 of the embryonic neural tube (Voiculescu et al., 2000), while the *Hoxb1*^{Cre} line drives expression in the rhombencephalon distal to the posterior border of rhombomere 3 (Arenkiel et al., 2003). We verified these expression patterns and demonstrated that cells derived from these lineages populate different regions of the adult cochlear nucleus (CN) and accessory auditory nuclei (AAN) (SUPPLEMENTAL FIGURE 1A–H). Virtually all neurons of the anteroventral cochlear nucleus (AVCN) and AAN are descended from the *Egr2* lineage, as are large neurons of the posteroventral (PVCN) and dorsal (DCN) cochlear nuclei (SUPPLEMENTAL FIGURE 1B–D). In contrast, the *Hoxb1* lineage densely populates the PVCN and DCN but contributes very few neurons to the AVCN (SUPPLEMENTAL FIGURE 1F, G). The majority of the AAN is also derived from the *Hoxb1* lineage with the exception of the medial nucleus of the trapezoid body (MNTB), where only about half of the neurons are labeled (SUPPLEMENTAL FIGURE 1H). These data suggest that the AVCN is derived almost solely from rhombomere 3, the PVCN from rhombomeres 3 and 4, the DCN from rhombomeres 4 and 5, the MNTB from rhombomeres 3 and 5, and the rest of the AAN from rhombomere 5. This is in good agreement with previous fate maps of the mouse CN (Farago et al., 2006) and chick superior olivary complex (Marin and Puelles, 1995).

We next used these *Cre*-driver alleles to delete a floxed allele of *Atoh1* (*Atoh1*^{flox}) (Shroyer et al., 2007) in transgenic mice. *Cre* expression in both of these lines precedes *Atoh1* expression

by 0.5–1 day, and we verified that *Atoh1* expression was completely absent from the regions where Cre protein was produced (SUPPLEMENTAL FIGURE 1I–N). This suggests that the overall recombination efficiency was close to 100% in both lines. *Egr2; Atoh1^{CKO}* animals were born in the expected Mendelian ratio, had a normal lifespan, and did not display any overt morphological or behavioral phenotypes. *Hoxb1; Atoh1^{CKO}* animals were born in the expected Mendelian ratio, but roughly 50% of these animals died within 24–36 hours of birth.

We examined the CN of adult *Egr2; Atoh1^{CKO}* and *Hoxb1; Atoh1^{CKO}* animals for morphological abnormalities. *Egr2; Atoh1^{CKO}* animals lack nearly the entire AVCN with the exception of a small portion of the posterior region, and both the DCN and PVCN are small compared to wildtype animals (FIGURE 1B, E, H; SUPPLEMENTAL FIGURE 2). In contrast, the AVCN is completely preserved in *Hoxb1; Atoh1^{CKO}* animals, but the majority of the PVCN and DCN are lost (FIGURE 1C, F, I; SUPPLEMENTAL FIGURE 3). Cochlear root neurons are absent from adult *Egr2; Atoh1^{CKO}* and *Hoxb1; Atoh1^{CKO}* animals (SUPPLEMENTAL FIGURES 2, 3). This pattern of neuronal loss corresponds to the areas of highest *Cre* expression in these *Cre*-driver lines and substantiates the proposed rhombomeric origins of the CN (SUPPLEMENTAL FIGURE 1B, C, F, G).

We performed immunocytochemistry for RORα, which is expressed by cartwheel cells in the DCN (Ino, 2004), and Cat-301, a marker of the extrasynaptic neuronal surface expressed throughout the AVCN and PVCN (Lurie et al., 1997), to more accurately identify the missing regions of the disrupted CN of *Atoh1^{CKO}* animals. RORα-positive and Cat-301-positive neurons are present in the CN of *Egr2; Atoh1^{CKO}* and *Hoxb1; Atoh1^{CKO}* animals (FIGURE 1J–O). These data demonstrate that no subdivision of the CN is completely lost in either of these *Atoh1^{CKO}* lines.

Accessory auditory neurons are lost in *Egr2; Atoh1^{CKO}* and *Hoxb1; Atoh1^{CKO}* animals due to primary and secondary effects of *Atoh1* loss

Given the disruption of CN structure, we hypothesized that output from the CN would also be disrupted. To assess this possibility, we examined the size of the trapezoid body, or ventral acoustic stria, a fiber tract that projects from the CN to the brainstem AAN. Nissl-stained sections of and lipophilic dye injections directly into the trapezoid body demonstrate that it is of reduced caliber in *Egr2; Atoh1^{CKO}* and *Hoxb1; Atoh1^{CKO}* animals, but that this reduction is much more dramatic in *Egr2; Atoh1^{CKO}* animals (single arrows in FIGURE 2A–C). In addition, dye injections into the trapezoid body failed to back-label CN neurons of *Egr2; Atoh1^{CKO}* mice, suggesting that these fibers do not originate from or connect to the CN (FIGURE 2B). Finally, dye injections into the CN of *Egr2; Atoh1^{CKO}* animals labeled cochlear afferents, but failed to label the trapezoid body or AAN (data not shown). These results suggest that the cellular disruption in the CN of *Hoxb1; Atoh1^{CKO}* mice reduces the projection to the AAN, and completely ablates this projection in *Egr2; Atoh1^{CKO}* animals.

The brainstem AAN, comprised of the superior olivary complex (SOC) and nuclei of the trapezoid body (NTB), are major targets of the CN. We therefore examined the morphology of these regions for possible secondary affects of CN disruption. The lateral superior olive (LSO), medial superior olive (MSO) and medial NTB (MNTB) are dramatically smaller in *Egr2; Atoh1^{CKO}* compared to wildtype animals, while more subtle decreases in size of the lateral NTB (LNTB) and ventral NTB (VNTB) are also present (FIGURE 2D, E, G, H; SUPPLEMENTAL FIGURE 4). In contrast, the effects on the AAN of *Hoxb1; Atoh1^{CKO}* animals are much less dramatic, with qualitative evidence of cell loss visible only in the LSO and MSO (FIGURE 2F, I; SUPPLEMENTAL FIGURE 4). The superior periolivary nucleus (SPN) is not affected in either *Atoh1^{CKO}* line.

The olivocochlear bundle (OCB) is the main efferent pathway to the cochlea. In rodents, choline acetyltransferase (ChAT)-positive neurons of the LNTB, LSO and VNTB project in the OCB (Yao and Godfrey, 1998). Since neurons in these regions are lost in *Egr2; Atoh1*^{CKO} and *Hoxb1; Atoh1*^{CKO} animals, we sought to determine if olivocochlear neurons were affected. ChAT-positive neurons are found in the regions of the LNTB, LSO and VNTB of *Egr2; Atoh1*^{CKO} and *Hoxb1; Atoh1*^{CKO} animals, but are more densely packed and located more ventrally than in wildtype animals (FIGURE 2J–L). These data demonstrate that the efferent auditory connections to the cochlea are not dependent upon connectivity with the CN for their survival.

The AAN lie within the domains of *Egr2*^{Cre} and *Hoxb1*^{Cre} expression (SUPPLEMENTAL FIGURE 1D, H), opening the possibility that primary deletion of *Atoh1* from this region could directly result in loss of neurons. Preliminary fate mapping data from our laboratory suggested that a population of SOC neurons that express the vesicular glutamate transporter VGLUT2 were derived from an early (E9.5 – E10.5) *Atoh1*-expressing lineage, and that these neurons were lost in *Atoh1*-null mice (HYZ, submitted). No *Atoh1*-lineal neurons labeled from E11.5 – E14.5 populated the AAN (data not shown). We used a tamoxifen-inducible system to fate map these cells in *Atoh1*$^{CreER\text{-}T2}$; *ROSA*^{R26R} mice and verified that a subset of neurons that populate the LSO and MSO were indeed descended from the *Atoh1* lineage (FIGURE 2M). *In situ* hybridization for *VGLUT2* on sections of the AAN from E18.5 *Egr2; Atoh1*^{CKO} animals shows that these neurons are missing, suggesting a primary effect of *Atoh1* loss on this neuronal population (FIGURE 2N, O). Neurons in other regions of the AAN are not descended from the *Atoh1* lineage, suggesting that loss of neurons in these areas must be secondary to deletion of *Atoh1* from the CN, LSO and/or MSO neurons.

Egr2; Atoh1^{CKO} and *Hoxb1; Atoh1*^{CKO} mice are deaf

We next sought to characterize the behavioral and physiological effects caused by disruptions of the central auditory system in *Atoh1*^{CKO} mice. We used the acoustic startle response to test hearing in *Egr2; Atoh1*^{CKO} and *Hoxb1; Atoh1*^{CKO} mice. Mice were placed in a small Plexiglas chamber where a piezoelectric device detected their movement in response to sounds of varying intensities. *Hoxb1; Atoh1*^{CKO} mice demonstrated no response to sounds of 120 dB (n=7, no stim vs 120 dB, t-test p = 0.36). *Egr2; Atoh1*^{CKO} animals responded to sounds of 120dB (n=15, no stim vs. 120dB, t-test p = 0.006), but this response was greatly attenuated when compared to littermate controls (inter-genotype comparison, ANOVA p = 0.0002, least-squares difference for pairwise comparisons p = 0.00002 to 0.33 for *Egr2; Atoh1*^{CKO} vs. other genotypes). Thus, *Egr2; Atoh1*^{CKO} and *Hoxb1; Atoh1*^{CKO} mice are behaviorally deaf.

To uncover the underlying auditory system defects, we performed electrophysiological testing of cochlear hair cell, auditory nerve and brainstem auditory pathway function. We measured distortion product otoacoustic emissions (DPOAEs), sounds generated secondary to non-linearities associated with outer hair cell force production, to examine forward and reverse transduction in *Atoh1*^{CKO} mice. *Hoxb1; Atoh1*^{CKO} animals had no measurable DPOAEs at any frequency or sound intensity tested, suggesting that defects in the peripheral auditory system are sufficient to explain their deafness. In contrast, DPOAEs and cochlear microphonics (CM), which are field potentials representing outer hair cell receptor potentials in response to acoustic stimuli, were normal in *Egr2; Atoh1*^{CKO} mice (FIGURE 3A, B). This demonstrates that hair cell function is normal in *Egr2; Atoh1*^{CKO} animals.

We next tested auditory nerve function in *Egr2; Atoh1*^{CKO} mice by recording compound action potentials (CAPs), field potentials generated by the synchronized firing of SGNs in response to tone burst stimuli (FIGURE 3C, E). CAPs with normal waveform morphology (FIGURE 3E) but slight decreases in amplitude were found in *Egr2; Atoh1*^{CKO} mice (FIGURE 3C, t-test *p = 0.05). Together with the normal hair cell function testing, these data suggest that defects

in the peripheral auditory system are insufficient to explain the profound hearing impairment of *Egr2; Atoh1*^{CKO} mice.

In contrast, we found that the auditory brainstem evoked response (ABR), consisting of synchronized field potentials generated by the auditory nerve and brainstem neurons in response to acoustic stimuli, had threshold elevations of 34–53dB (mean = 44dB) across all frequencies tested and showed loss of the later waveforms generated by the brainstem auditory pathways (FIGURE 3D, E). These findings show that sound information does not propagate beyond the auditory nerve. Together with the histological findings, these data demonstrate that CN dysfunction causes the deafness seen in *Egr2; Atoh1*^{CKO} mice.

Spiral ganglion cells are lost in *Egr2; Atoh1*^{CKO} animals despite normal cochlear structure and hair cell morphology

Atoh1 is necessary for the development of inner ear hair cells (Bermingham et al., 1999). To be certain that *Atoh1* was not deleted from this cell population, we carefully analyzed the structure of *Egr2; Atoh1*^{CKO} mouse cochleae (FIGURE 4). The overall structure of the cochlea is unchanged in *Egr2; Atoh1*^{CKO} animals, where a continuous line of *Atoh1*-expressing hair cells is present in all turns of the cochlea at birth (FIGURE 4A, B). In addition, both inner and outer hair cell morphology is preserved throughout all cochlear turns, as demonstrated by representative sections from the mid-modiolar region of adult cochleae shown in FIGURE 4C–F. These data, combined with normal hair cell electrophysiological data, suggest that the hair cell population is not affected in *Egr2; Atoh1*^{CKO} animals. The cochlear hair cell population of *Hoxb1; Atoh1*^{CKO} mice, however, was not normal (data not shown); further studies of these abnormalities will be the subject of another report. Based on the potential complex interactions of primary peripheral and central effects on the auditory system of *Hoxb1; Atoh1*^{CKO} mice, the rest of the present report will focus on further characterization of *Egr2; Atoh1*^{CKO} animals.

We were surprised to find that SGNs and their axons were missing from P18 and adult *Egr2; Atoh1*^{CKO} cochleae (FIGURE 5A–C). Quantification of SGN soma (means: 10,258 neurons in *Egr2*$^{+/+}$*; Atoh1*$^{+/flox}$ vs. 7,094 neurons in *Egr2; Atoh1*^{CKO}, t-test p = 0.01) and axon numbers (means: base, 70 axons in *Egr2*$^{+/+}$*; Atoh1*$^{+/flox}$ vs. 48 axons in *Egr2; Atoh1*^{CKO}, t-test p = 0.09; middle, 247 axons in *Egr2*$^{+/+}$*; Atoh1*$^{+/flox}$ vs. 148 axons in *Egr2; Atoh1*^{CKO}, t-test p = 0.004) in the cochlea and auditory nerve demonstrated a 30% reduction in *Egr2; Atoh1*^{CKO} animals (FIGURE 5C). This reduction in SGN and auditory nerve fiber numbers probably accounts for the decreased CAP amplitude found in *Egr2; Atoh1*^{CKO} mice (FIGURE 3C). SGN numbers in wildtype animals with one copy of the *Egr2*^{Cre} or *Atoh1*^{LacZ} allele were normal (*Egr2*$^{+/+}$*; Atoh1*$^{+/flox}$ vs. *Egr2*$^{Cre/+}$*; Atoh1*$^{+/flox}$ vs. *Egr2*$^{+/+}$*; Atoh1*$^{LacZ/flox}$; ANOVA p=0.21), demonstrating that this effect was specific to conditional deletion of *Atoh1*.

Atoh1 is expressed by postnatal SGNs, although its role in this cell population is unclear (Matei et al., 2005). To rule out a direct effect of *Atoh1* deletion on SGNs, we fate-mapped *Egr2*-lineal cells in the cochlea of adult *Egr2*^{Cre}; *ROSA*^{R26R} animals (FIGURE 5D–D″). Double immunolabeling for β-galactosidase and a neuronal marker (TuJ1) demonstrated that the two antigens have non-overlapping expression patterns in the spiral ganglion. These data show that, as expected, *Egr2*^{Cre} was expressed only by Schwann cells of the spiral ganglion. Although it has never been demonstrated in any region of the central or peripheral nervous systems, it is also possible that *Atoh1* could be expressed by glial cells of the SG and is somehow necessary for their survival. Glial cells are present in SGs of adult and early postnatal *Egr2; Atoh1*^{CKO} animals (FIGURE 6C, D), demonstrating that deleterious effects of *Atoh1* loss on this cell population cannot explain SGN loss. Thus, loss of *Atoh1* expression from the spiral ganglion is not the cause of the decreased SGN number seen in *Egr2; Atoh1*^{CKO} cochleae.

We next examined the central auditory nerve projection using lipophilic dyes to determine if SGN axons projected appropriately to the CN. At P0, robust projections normally connect the apex (green) and base (red) to the DCN and VCN (FIGURE 5E, G). Axon bundles of the central projection to the VCN are reduced in size in P0 *Egr2; Atoh1*^{CKO} animals, and the axons of the auditory nerve fibers defasciculate and project aberrantly in both the rostral and caudal dimensions (FIGURE 5F, H). These data, along with the SGN counts, suggest that the deletion of *Atoh1*-lineal cells from the CN of *Egr2; Atoh1*^{CKO} animals causes secondary loss of SGNs and their axons, and aberrant projection of the remaining auditory nerve fibers.

Neuronal loss in the SG and AAN occurs between P0 and P3, revealing a novel critical period

If the neuronal loss in the peripheral and central auditory systems is in fact secondary to a failure in genesis of CN and SOC neurons, there should be a time period at which the SGN, LNTB, MNTB and VNTB neuronal populations are normal in appearance. We therefore examined the morphology of the SGN and AAN of *Egr2; Atoh1*^{CKO} animals and counted the number of neurons in these structures at different postnatal times. SGs of *Egr2; Atoh1*^{CKO} mice were normal in appearance and neuron number at P0, but by P3 the number of neurons dropped to 70% of the wildtype value (FIGURE 6A, B, E). Similarly, the LNTB, MNTB and VNTB of *Egr2; Atoh1*^{CKO} animals appeared qualitatively normal at P0, but showed loss of neurons by P3 (FIGURE 6F–I). Quantification of MNTB neurons (chosen because the nucleus is easily identifiable at all postnatal ages) revealed no difference between wildtype and *Egr2; Atoh1*^{CKO} animals at P0 (t-test, p=0.43). However, neuronal number decreased to 50% of the wildtype value at P3, and to ~30% at P7 and in adulthood (FIGURE 6J). In addition, there was a 7-fold increase in cell death (as measured by the number of pyknotic nuclei) in the MNTB of P3 *Egr2; Atoh1*^{CKO} compared to wildtype animals, but no difference at P0 or P7 (FIGURE 6K). These data identify a critical period between P0 and P3 during which the SGN and MNTB neuronal populations require contact with CN neurons for their survival.

DISCUSSION

Secondary dependence of SG and AAN neurons on *Atoh1*-lineal neurons

The most novel finding of our study is that the survival of a subset of neurons in the SG and AAN depends upon *Atoh1*-lineal neurons in the central auditory system during a well-defined developmental time period coincident with the first three days of postnatal life. This critical period is not concomitant with or an extension of any previously reported period of naturally occurring cell death in these populations. This observation adds to the evidence for a complex interdependence of peripheral and central auditory system neurons that changes during developmental time.

Our data suggest that the majority of AAN neuronal loss in *Atoh1*^{CKO} animals is a secondary effect of disruption of the AVCN. Primary deletion of *Atoh1* from the LSO and MSO should occur to a similar extent in *Egr2; Atoh1*^{CKO} and *Hoxb1; Atoh1*^{CKO} animals since these nuclei are derived from rhombomere 5, yet loss of neurons from AAN subnuclei not derived from the *Atoh1* lineage (LNTB, MNTB, and VNTB) occurs only in *Egr2; Atoh1*^{CKO} animals. In addition, the magnitude of neuronal loss from the LSO and MSO themselves is much greater in *Egr2; Atoh1*^{CKO} than *Hoxb1; Atoh1*^{CKO} animals. These findings are consistent with the fact that the AVCN provides the majority of afferents to the LNTB, LSO, MNTB and MSO (Harrison and Irving, 1966; Willott, 2001). These data are surprising given that they suggest that deafferentation of AAN neurons rather than loss of target is what leads to their demise; possible reasons for this are discussed in the next section.

Lesions of the AVCN and cochlear nerve cause substantial loss (up to 95%) of SGNs in adult animals, suggesting that the mature SGN population must maintain central connectivity to

remain viable (Spoendlin, 1971; Leake et al., 1992; Sekiya et al., 2003). However, interpretation of these studies is difficult because damage to SGN axons and/or the cochlear blood supply occurs and probably contributes to the neuronal loss. No experiments prior to our own have attempted to assess the dependency of the mammalian SGN population on central connectivity during early postnatal development.

In contrast to peripheral lesions, the effects of central deafferentation depend upon the age of the animal. In adult animals, cochlear ablation results only in decreased soma size and dendritic arborization, but no cell loss, in the CN and AAN (Powell and Erulkar, 1962; Pasic et al., 1994). Cochlear ablation prior to the onset of hearing, however, causes neuronal death in the ipsilateral VCN and LSO (Trune, 1982; Moore, 1990, 1992), but not until the age of hearing onset. This suggests that a critical period concomitant with the initiation of sensory-evoked activity exists in these neuronal populations. The secondary neuronal loss that we observe in the AAN of *Egr2; Atoh1*^{CKO} mice precedes the onset of hearing by more than one week, which occurs between P11 and P15 in mice (Friauf and Lohmann, 1999). This suggests that a mechanism independent of sensory-evoked activity is responsible for the secondary neuronal loss. We propose that this mechanism involves neurotrophin signaling.

Proposed mechanisms for neuronal loss

Neuronal death in the SG and AAN of *Egr2; Atoh1*^{CKO} mice could be secondary to the loss of trophic factors normally supplied by the AVCN. BDNF, Ntf3 and their receptors (Ntrk2 and Ntrk3, respectively) are expressed during embryonic and early postnatal development in the cochlea and in regions of the auditory brainstem (Ylikoski et al., 1993; Schecterson and Bothwell, 1994; Hafidi et al., 1996; Pirvola et al., 1997). Both neurotrophins are necessary for maintenance of the SGN population, as Ntf3 null mice lose about 85%, BDNF null mice lose 7–15%, and BDNF/Ntf3 double-null mice lose all of their SGNs (Jones et al., 1994; Ernfors et al., 1995; Rubel and Fritzsch, 2002). Combined disruption of the cognate BDNF and Ntf3 receptors (Ntrk2 and Ntrk3, respectively) also results in complete loss of SGNs (Silos-Santiago et al., 1997), and incomplete deficiencies of these receptors lead to variable amounts of regional SGN loss (Fritzsch et al., 1998). In the AAN, an unusual twist in this scenario is that the trophic support would have to occur in an anterograde rather than retrograde fashion. There is precedence for this phenomenon, as anterograde actions of Ntf3 have been described in the central nervous system, primarily in the visual system (von Bartheld et al., 1996; Wang et al., 2002; Butowt and von Bartheld, 2005; von Bartheld and Fritzsch, 2006).

Other trophic influences could also be involved in the maintenance of neurons in the SG and AAN. For instance, the ablation of the CN could negatively impact the propagation of spontaneous activity between these regions. Spontaneous activity in the developing auditory system begins during embryogenesis (Lippe, 1994; Jones et al., 2001), but its role in development and trophism in these cell populations remains unknown. However, spontaneous activity has been demonstrated to be important for the correct differentiation and maintenance of neuronal subclasses in other regions of the central nervous system (Hanson and Landmesser, 2004). Other forms of trophism stemming from direct neuronal contact might also be important for the maintenance of these cell populations. Further experiments are necessary to determine the relative contributions of these potential trophic interactions on the developing auditory system.

Evolutionary conservation of *Atoh1* function

Our data provide further support for the evolutionary conservation of *Atoh1* function in the organization of the auditory system as a whole. In *Drosophila*, *atonal* is necessary and sufficient for specifying sensory neurons found in chordotonal organs (CHOs), which act as proprioceptors in the fly cuticle (Jarman et al., 1993). An array of CHOs make up Johnston's

organ, a structure in the second antennal segment that is specialized for hearing; *atonal*-null flies lack this structure and are subsequently deaf. In mammals, there is recent evidence that *Atoh1* may be expressed at low levels in a subset of SGNs (Matei et al., 2005), although the role this expression plays in this cell population is unknown. In contrast, *Atoh1* is highly expressed by inner ear hair cells (which detect the auditory signal) and by neurons of the CN, LSO and MSO. These cell groups contribute to the afferent auditory pathway, require *Atoh1* for their specification, and their presence is necessary for SGN survival. In addition, we show that brainstem AAN neurons depend upon the presence of *Atoh1*-lineal neurons in the CN for their maintenance. So, although the sites of *Atoh1* expression have changed through evolutionary time, the gene is still required for the organization of both the peripheral and central auditory pathways.

In summary, we demonstrate that conditional deletion of *Atoh1* from rhombomeres 3–5 results directly in deletion of neurons from the CN, LSO and MSO and in secondary loss of neurons in the SG and brainstem AAN. Thus, *Egr2; Atoh1*^{CKO} and *Hoxb1; Atoh1*^{CKO} mice represent novel model systems to examine perturbations of the central auditory system. Our findings may have relevance for understanding the extent to which malformations of and/or prenatal insults to the brainstem in human patients impair hearing, and may help to provide insight into why cochlear implants in these patients sometimes prove unsuccessful.

Supplementary Material

Refer to Web version on PubMed Central for supplementary material.

Acknowledgments

We thank Drs. Patrick Charnay (*Egr2*^{Cre}) and Mario Capecchi (*Hoxb1*^{Cre}) for generously sharing mouse lines with us; Dr. William Brownell, Dr. Sharyl Fyffe and members of the Zoghbi lab for thoughtful discussions of the data and critical reading of this manuscript; and Bobbie Antalffy, Nancy Ao, Gabrielle Schuster and Sukeshi Vaishnav for technical assistance. Mouse behavior testing was supported by the Baylor MRDDRC Neurobehavioral Core; *in situ* hybridization was done by the Baylor MRDDRC *In Situ* Hybridization Core (NIH HD024064); and confocal work was done at the Baylor MRDDRC Imaging Core, Case Western Reserve University Neurosciences Imaging Center, and at Creighton University in part through a gift from the Roy J. Carver foundation to BF. SMM is funded by NIH K08NS053419, JSO by NIH K08DC006671, BF by NIH R01DC005590, and HYZ is an investigator in the Howard Hughes Medical Institute.

References

Agrawal Y, Platz EA, Niparko JK. Prevalence of hearing loss and differences by demographic characteristics among US adults: data from the National Health and Nutrition Examination Survey, 1999–2004. Arch Intern Med 2008;168:1522–1530. [PubMed: 18663164]

Akazawa C, Ishibashi M, Shimizu C, Nakanishi S, Kageyama R. A mammalian helix-loop-helix factor structurally related to the product of Drosophila proneural gene atonal is a positive transcriptional regulator expressed in the developing nervous system. J Biol Chem 1995;270:8730–8738. [PubMed: 7721778]

Arenkiel BR, Gaufo GO, Capecchi MR. Hoxb1 neural crest preferentially form glia of the PNS. Dev Dyn 2003;227:379–386. [PubMed: 12815623]

Ben-Arie N, McCall AE, Berkman S, Eichele G, Bellen HJ, Zoghbi HY. Evolutionary conservation of sequence and expression of the bHLH protein Atonal suggests a conserved role in neurogenesis. Hum Mol Genet 1996;5:1207–1216. [PubMed: 8872459]

Bermingham NA, Hassan BA, Price SD, Vollrath MA, Ben-Arie N, Eatock RA, Bellen HJ, Lysakowski A, Zoghbi HY. Math1: an essential gene for the generation of inner ear hair cells. Science 1999;284:1837–1841. [PubMed: 10364557]

Butowt R, von Bartheld CS. Anterograde axonal transport of BDNF and NT-3 by retinal ganglion cells: roles of neurotrophin receptors. Mol Cell Neurosci 2005;29:11–25. [PubMed: 15866043]

Cambronero F, Puelles L. Rostrocaudal nuclear relationships in the avian medulla oblongata: a fate map with quail chick chimeras. J Comp Neurol 2000;427:522–545. [PubMed: 11056462]

Carson JP, Thaller C, Eichele G. A transcriptome atlas of the mouse brain at cellular resolution. Curr Opin Neurobiol 2002;12:562–565. [PubMed: 12367636]

Carson JP, Eichele G, Chiu W. A method for automated detection of gene expression required for the establishment of a digital transcriptome-wide gene expression atlas. J Microsc 2005;217:275–281. [PubMed: 15725131]

Cramer KS, Fraser SE, Rubel EW. Embryonic origins of auditory brain-stem nuclei in the chick hindbrain. Dev Biol 2000;224:138–151. [PubMed: 10926755]

Ernfors P, Van De Water T, Loring J, Jaenisch R. Complementary roles of BDNF and NT-3 in vestibular and auditory development. Neuron 1995;14:1153–1164. [PubMed: 7605630]

Farago AF, Awatramani RB, Dymecki SM. Assembly of the brainstem cochlear nuclear complex is revealed by intersectional and subtractive genetic fate maps. Neuron 2006;50:205–218. [PubMed: 16630833]

Friauf E, Lohmann C. Development of auditory brainstem circuitry. Activity-dependent and activity-independent processes. Cell Tissue Res 1999;297:187–195. [PubMed: 10470488]

Fritzsch B, Barbacid M, Silos-Santiago I. The combined effects of trkB and trkC mutations on the innervation of the inner ear. Int J Dev Neurosci 1998;16:493–505. [PubMed: 9881298]

Fritzsch B, Muirhead KA, Feng F, Gray BD, Ohlsson-Wilhelm BM. Diffusion and imaging properties of three new lipophilic tracers, NeuroVue Maroon, NeuroVue Red and NeuroVue Green and their use for double and triple labeling of neuronal profile. Brain Res Bull 2005;66:249–258. [PubMed: 16023922]

Griffiths TD. Central auditory pathologies. Br Med Bull 2002;63:107–120. [PubMed: 12324387]

Hafidi A, Moore T, Sanes DH. Regional distribution of neurotrophin receptors in the developing auditory brainstem. J Comp Neurol 1996;367:454–464. [PubMed: 8698904]

Hanson MG, Landmesser LT. Normal patterns of spontaneous activity are required for correct motor axon guidance and the expression of specific guidance molecules. Neuron 2004;43:687–701. [PubMed: 15339650]

Harrison JM, Irving R. Ascending connections of the anterior ventral cochlear nucleus in the rat. J Comp Neurol 1966;126:51–63. [PubMed: 5935369]

Hendry IA. A method to correct adequately for the change in neuronal size when estimating neuronal numbers after nerve growth factor treatment. J Neurocytol 1976;5:337–349. [PubMed: 939967]

Ino H. Immunohistochemical characterization of the orphan nuclear receptor ROR alpha in the mouse nervous system. J Histochem Cytochem 2004;52:311–323. [PubMed: 14966198]

Jarman AP, Grau Y, Jan LY, Jan YN. atonal is a proneural gene that directs chordotonal organ formation in the Drosophila peripheral nervous system. Cell 1993;73:1307–1321. [PubMed: 8324823]

Jones KR, Farinas I, Backus C, Reichardt LF. Targeted disruption of the BDNF gene perturbs brain and sensory neuron development but not motor neuron development. Cell 1994;76:989–999. [PubMed: 8137432]

Jones TA, Jones SM, Paggett KC. Primordial rhythmic bursting in embryonic cochlear ganglion cells. J Neurosci 2001;21:8129–8135. [PubMed: 11588185]

Leake PA, Snyder RL, Merzenich MM. Topographic organization of the cochlear spiral ganglion demonstrated by restricted lesions of the anteroventral cochlear nucleus. J Comp Neurol 1992;320:468–478. [PubMed: 1629399]

Lippe WR. Rhythmic spontaneous activity in the developing avian auditory system. J Neurosci 1994;14:1486–1495. [PubMed: 8126550]

Lurie DI, Pasic TR, Hockfield SJ, Rubel EW. Development of Cat-301 immunoreactivity in auditory brainstem nuclei of the gerbil. J Comp Neurol 1997;380:319–334. [PubMed: 9087516]

Machold R, Fishell G. Math1 is expressed in temporally discrete pools of cerebellar rhombic-lip neural progenitors. Neuron 2005;48:17–24. [PubMed: 16202705]

Marin F, Puelles L. Morphological fate of rhombomeres in quail/chick chimeras: a segmental analysis of hindbrain nuclei. Eur J Neurosci 1995;7:1714–1738. [PubMed: 7582126]

Matei V, Pauley S, Kaing S, Rowitch D, Beisel KW, Morris K, Feng F, Jones K, Lee J, Fritzsch B. Smaller inner ear sensory epithelia in Neurog 1 null mice are related to earlier hair cell cycle exit. Dev Dyn 2005;234:633–650. [PubMed: 16145671]

Moore DR. Auditory brainstem of the ferret: early cessation of developmental sensitivity of neurons in the cochlear nucleus to removal of the cochlea. J Comp Neurol 1990;302:810–823. [PubMed: 2081818]

Moore DR. Trophic influences of excitatory and inhibitory synapses on neurones in the auditory brain stem. Neuroreport 1992;3:269–272. [PubMed: 1515583]

Pasic TR, Moore DR, Rubel EW. Effect of altered neuronal activity on cell size in the medial nucleus of the trapezoid body and ventral cochlear nucleus of the gerbil. J Comp Neurol 1994;348:111–120. [PubMed: 7814680]

Pirvola U, Hallbook F, Xing-Qun L, Virkkala J, Saarma M, Ylikoski J. Expression of neurotrophins and Trk receptors in the developing, adult, and regenerating avian cochlea. J Neurobiol 1997;33:1019–1033. [PubMed: 9407020]

Postigo A, Calella AM, Fritzsch B, Knipper M, Katz D, Eilers A, Schimmang T, Lewin GR, Klein R, Minichiello L. Distinct requirements for TrkB and TrkC signaling in target innervation by sensory neurons. Genes Dev 2002;16:633–645. [PubMed: 11877382]

Powell TP, Erulkar SD. Transneuronal cell degeneration in the auditory relay nuclei of the cat. J Anat 1962;96:249–268. [PubMed: 14488390]

Rubel EW, Fritzsch B. Auditory system development: primary auditory neurons and their targets. Annu Rev Neurosci 2002;25:51–101. [PubMed: 12052904]

Schecterson LC, Bothwell M. Neurotrophin and neurotrophin receptor mRNA expression in developing inner ear. Hear Res 1994;73:92–100. [PubMed: 8157510]

Sekiya T, Yagihashi A, Shimamura N, Asano K, Suzuki S, Matsubara A, Namba A, Shinkawa H. Apoptosis of auditory neurons following central process injury. Exp Neurol 2003;184:648–658. [PubMed: 14769356]

Shroyer NF, Helmrath MA, Wang VY, Antalffy B, Henning SJ, Zoghbi HY. Intestine-specific ablation of mouse atonal homolog 1 (Math1) reveals a role in cellular homeostasis. Gastroenterology 2007;132:2478–2488. [PubMed: 17570220]

Silos-Santiago I, Fagan AM, Garber M, Fritzsch B, Barbacid M. Severe sensory deficits but normal CNS development in newborn mice lacking TrkB and TrkC tyrosine protein kinase receptors. Eur J Neurosci 1997;9:2045–2056. [PubMed: 9421165]

Soriano P. Generalized lacZ expression with the ROSA26 Cre reporter strain. Nat Genet 1999;21:70–71. [PubMed: 9916792]

Spoendlin H. Degeneration behaviour of the cochlear nerve. Arch Klin Exp Ohren Nasen Kehlkopfheilkd 1971;200:275–291. [PubMed: 5159190]

Trune DR. Influence of neonatal cochlear removal on the development of mouse cochlear nucleus: I. Number, size, and density of its neurons. J Comp Neurol 1982;209:409–424. [PubMed: 7130465]

Visel A, Thaller C, Eichele G. GenePaint.org: an atlas of gene expression patterns in the mouse embryo. Nucleic Acids Res 2004;32:D552–556. [PubMed: 14681479]

Voiculescu O, Charnay P, Schneider-Maunoury S. Expression pattern of a Krox-20/Cre knock-in allele in the developing hindbrain, bones, and peripheral nervous system. Genesis 2000;26:123–126. [PubMed: 10686605]

von Bartheld CS, Fritzsch B. Comparative analysis of neurotrophin receptors and ligands in vertebrate neurons: tools for evolutionary stability or changes in neural circuits? Brain Behav Evol 2006;68:157–172. [PubMed: 16912469]

von Bartheld CS, Byers MR, Williams R, Bothwell M. Anterograde transport of neurotrophins and axodendritic transfer in the developing visual system. Nature 1996;379:830–833. [PubMed: 8587607]

Wang VY, Rose MF, Zoghbi HY. Math1 expression redefines the rhombic lip derivatives and reveals novel lineages within the brainstem and cerebellum. Neuron 2005;48:31–43. [PubMed: 16202707]

Wang X, Butowt R, Vasko MR, von Bartheld CS. Mechanisms of the release of anterogradely transported neurotrophin-3 from axon terminals. J Neurosci 2002;22:931–945. [PubMed: 11826122]

Willott, J., editor. Handbook of Mouse Auditory Research: From Behavior to Molecular Biology. Boca Raton: CRC Press; 2001.

Xia A, Visosky AM, Cho JH, Tsai MJ, Pereira FA, Oghalai JS. Altered Traveling Wave Propagation and Reduced Endocochlear Potential Associated with Cochlear Dysplasia in the BETA2/NeuroD1 Null Mouse. J Assoc Res Otolaryngol 2007;8:447–463. [PubMed: 17701252]

Yao W, Godfrey DA. Immunohistochemical evaluation of cholinergic neurons in the rat superior olivary complex. Microsc Res Tech 1998;41:270–283. [PubMed: 9605344]

Yaylaoglu MB, Titmus A, Visel A, Alvarez-Bolado G, Thaller C, Eichele G. Comprehensive expression atlas of fibroblast growth factors and their receptors generated by a novel robotic in situ hybridization platform. Dev Dyn 2005;234:371–386. [PubMed: 16123981]

Ylikoski J, Pirvola U, Moshnyakov M, Palgi J, Arumae U, Saarma M. Expression patterns of neurotrophin and their receptor mRNAs in the rat inner ear. Hear Res 1993;65:69–78. [PubMed: 8080462]

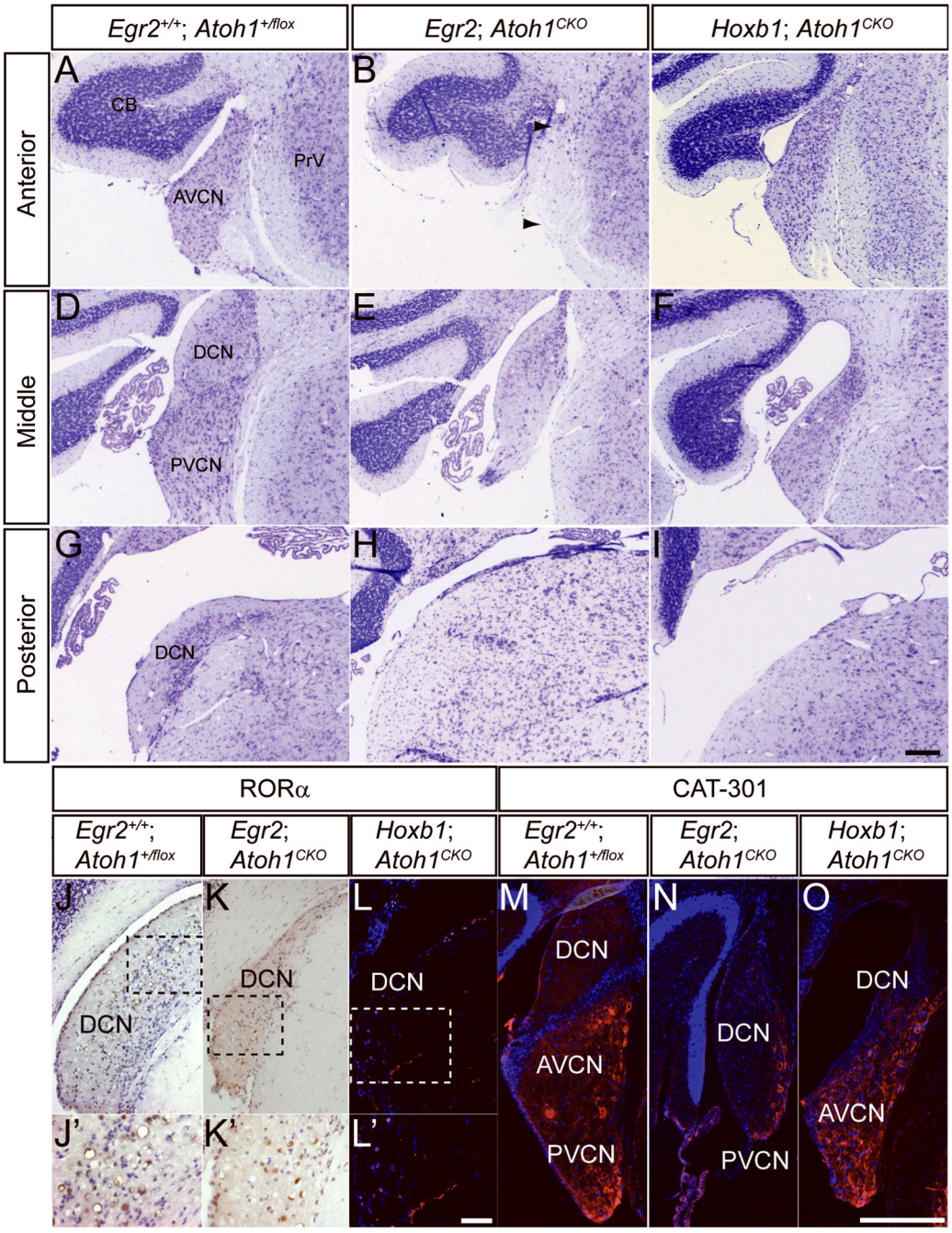

Figure 1.

Different subnuclei of the CN are disrupted in adult *Egr2; Atoh1*^{CKO} and *Hoxb1; Atoh1*^{CKO} mice. (A–I) Cresyl violet stained sections of CN from wildtype (A, D, G), *Egr2; Atoh1*^{CKO} (B, E, H) and *Hoxb1; Atoh1*^{CKO} (C, F, I) animals at anterior (A–C), middle (D–F) and posterior (G–I) levels. The AVCN is most severely affected in *Egr2; Atoh1*^{CKO} mice, although the auditory nerve fibers are preserved (B, arrows). The PVCN and DCN are most severely affected in *Hoxb1; Atoh1*^{CKO} animals. (J–L) RORα immunostaining of DCN from wildtype (J, J′), *Egr2; Atoh1*^{CKO} (K, K′) and *Hoxb1; Atoh1*^{CKO} (L, L′) animals. RORα-positive cells, which are present only in the DCN, are seen in all three genotypes. (J′–L′) Higher magnification views of boxed areas in J–L, respectively. (M–O) Cat-301 immunostaining is present in the VCN of

wildtype (M), *Egr2; Atoh1*^{CKO} (N) and *Hoxb1; Atoh1*^{CKO} (O) animals. Scale bars: (A–I, M–O) 200 μm, (J–L) 100 μm, (J′–L′) 12.5 μm.

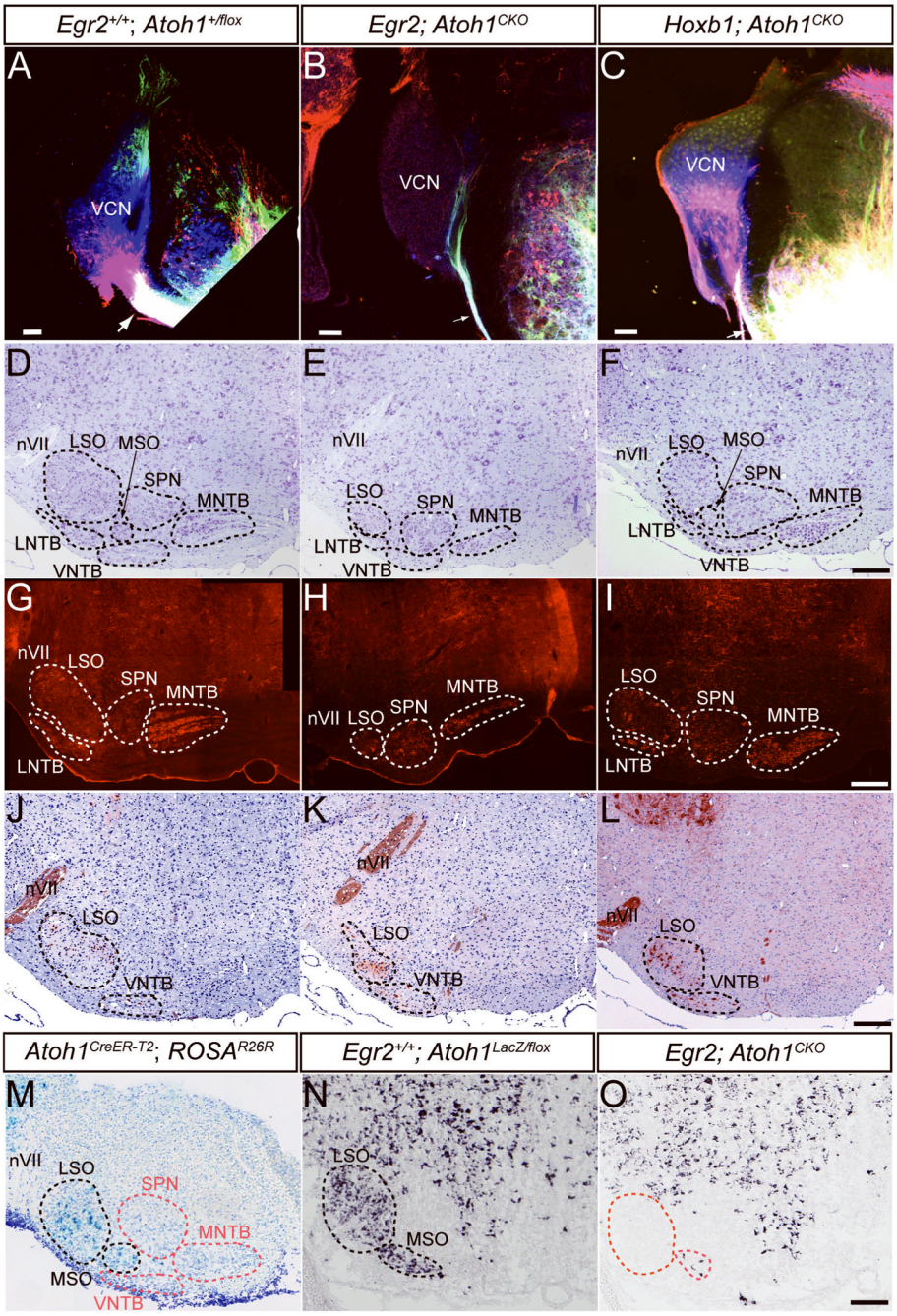

Figure 2.

The brainstem AAN and pathways are disrupted in *Egr2; Atoh1*^{CKO} and *Hoxb1; Atoh1*^{CKO} mice. (A–C) Lipophilic dye injections into the acoustic stria at P18 retrogradely label the CN of wildtype and *Hoxb1; Atoh1*^{CKO} (A, C) but not *Egr2; Atoh1*^{CKO} (B) animals. NeuroVue dyes were injected into the ventral acoustic stria near the facial nerve (red) and trigeminal nerve (blue), and into the dorsal and ventral acoustic stria between the other two injections (green). Note the massive filling of the ventral acoustic stria and retrograde filling of DCN (green cells) and VCN (blue and red cells) in wildtype (A) and *Hoxb1; Atoh1*^{CKO} (C) mice. The caliber of the ventral acoustic stria is much smaller in *Egr2; Atoh1*^{CKO} animals (compare single arrows in A–C), showing only fibers projecting into the ventral cochlear nucleus that may represent

inferior colliculus, superior olive or trigeminal fibers known to reach the CN in mice. The ventral acoustic stria is also reduced in size in *Hoxb1; Atoh1*^{CKO} mice (arrow), but retrogradely labeled neurons are still found throughout the CN. For the remaining panels, sections from similar anteroposterior levels of the brainstem are presented for each of the genotypes. (D–F) Cresyl violet stain of AAN in 7 week old wildtype, *Egr2; Atoh1*^{CKO} and *Hoxb1; Atoh1*^{CKO} mice. The nuclear subdivisions are outlined and labeled. The LSO, MNTB, MSO and VNTB are reduced in size in *Egr2; Atoh1*^{CKO} animals (E), while only the LSO appears to be affected in *Hoxb1; Atoh1*^{CKO} animals (F). (G–I) Cat-301 immunostaining of accessory auditory nuclei shows loss of neurons from the LNTB, LSO, and MNTB of *Egr2; Atoh1*^{CKO} animals, and cell loss from only the LSO of *Hoxb1; Atoh1*^{CKO} animals. (J–L) Choline acetyltransferase (ChAT) immunostaining of brainstems from wildtype, *Egr2; Atoh1*^{CKO} and *Hoxb1; Atoh1*^{CKO} mice confirms that, in all genotypes, neurons in the LSO and VNTB that project in the olivocochlear bundle are present. Note the increased packing density and different positions of these neurons in the LSO of *Egr2; Atoh1*^{CKO} and *Hoxb1; Atoh1*^{CKO} compared to wildtype animals. (M) Xgal stain of AAN from E18.5 *Atoh1*$^{CreER\text{-}T2}$ embryo whose pregnant dam was injected with tamoxifen at E10.5. Labeled cells are found in the developing LSO and MSO (black dotted lines). AAN without labeled cells are designated by red dotted lines. (N, O) *VGLUT2 in situ* hybridization of brainstem sections from E18.5 wildtype (N) and *Egr2; Atoh1*^{CKO} (O) embryos. The wildtype distribution of *VGLUT2* mRNA in the AAN is virtually identical to the Xgal expression pattern in panel (M). Only a few *VGLUT2*-expressing cells are present in the LSO and MSO of the *Egr2; Atoh1*^{CKO} embryo, suggesting a primary effect of *Atoh1* deletion. Red dotted lines in panel (O) show the expected position of these cells. LNTB – lateral nucleus of the trapezoid body, LSO – lateral superior olive, MNTB – medial nucleus of the trapezoid body, MSO – medial superior olive, nVII – 7th nerve, SPN – superior periolivary nucleus, VCN – ventral cochlear nucleus, VNTB – ventral nucleus of the trapezoid body. Scale bars: (A, B, C) 100 μm, (D–O) 200 μm.

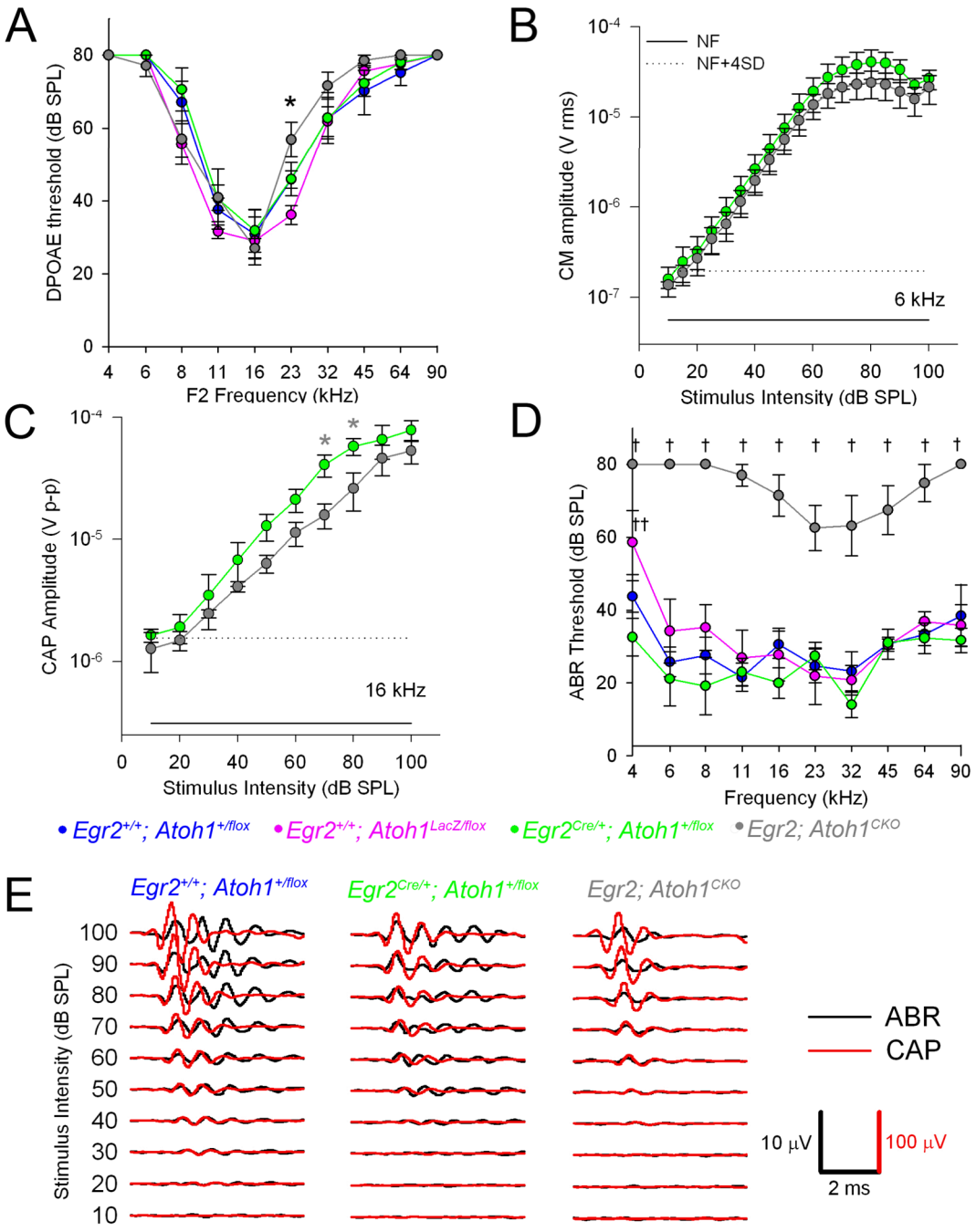

Figure 3.

Egr2; Atoh1^{CKO} mice have normal cochlear function but have mild auditory nerve and severe brainstem auditory pathway dysfunction. Data are plotted as mean ± SEM. (A) Distortion product otoacoustic emission (DPOAE) thresholds (n=6–9 animals per genotype). There is only one statistically significant difference at 23 kHz (ANOVA followed by least-squares difference for pairwise comparisons, *p = 0.032 for *Egr2; Atoh1*^{CKO} vs. *Egr2*$^{+/+}$*; Atoh1*$^{+/flox}$, and p = 0.0002 for *Egr2; Atoh1*^{CKO} vs. *Egr2*$^{+/+}$*; Atoh1*$^{LacZ/flox}$). (B) Cochlear microphonic (CM) amplitudes from *Egr2*$^{Cre/+}$*; Atoh1*$^{+/flox}$ (n=4) and *Egr2; Atoh1*^{CKO} animals (n=3). The solid line is the noise floor and the dotted line is the rms noise floor +4 SD. There were no statistically significant differences between the responses of the two genotypes at any

of the stimulus intensities tested. (C) Compound action potential (CAP) amplitudes from *Egr2*$^{Cre/+}$*; Atoh1*$^{+flox}$ (green circles, n=4) and *Egr2; Atoh1*^{CKO} (gray circles, n=3) mice. T-test *p = 0.05. CAP amplitudes were mildly reduced in *Egr2; Atoh1*^{CKO} mice relative to controls. Solid and dotted lines same as panel (B). (D) Auditory brainstem evoked response (ABR) thresholds (n=7–9 animals per genotype). ANOVA followed by least-squares differences †p< = 0.00000001 to 0.018 *Egr2; Atoh1*^{CKO} vs. others, ††p = 0.005 *Egr2*$^{Cre/+}$*; Atoh1*$^{+/flox}$ vs. *Egr2*$^{+/+}$*; Atoh1*$^{LacZ/flox}$. ABR thresholds were significantly elevated in *Egr2; Atoh1*^{CKO} mice relative to controls. (E) Representative ABR and CAP waveforms from single mice. The CAP waveforms (shown in red) are similar among the animals, confirming that the auditory nerve is receiving information from the inner hair cell appropriately. However, the ABR waveform (shown in black) in the *Egr2; Atoh1*^{CKO} animal is shorter in duration and has fewer peaks, suggesting that the signal is not propagated within the brainstem.

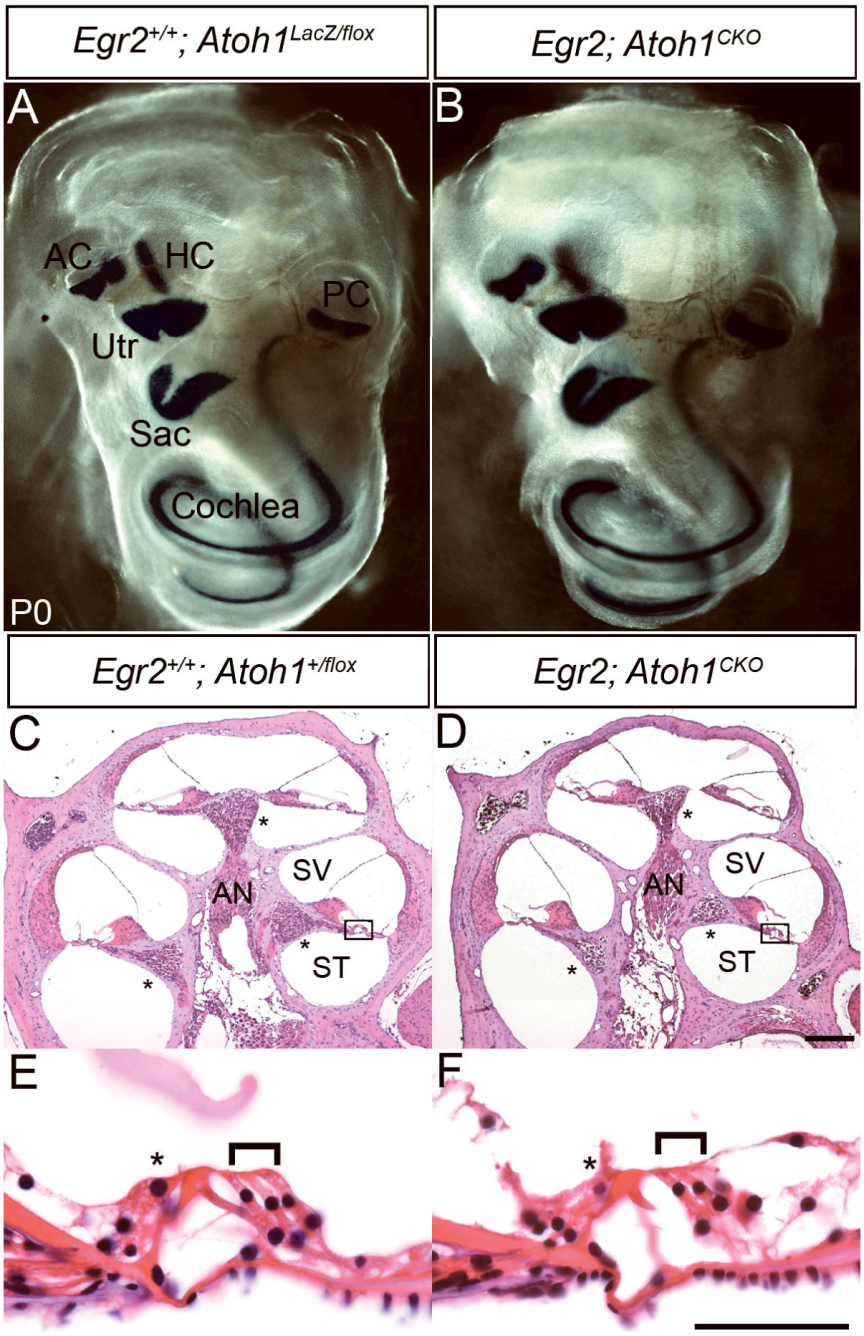

Figure 4.

The cochlea and organ of Corti are structurally normal in *Egr2; Atoh1*^{CKO} animals. (A) *Egr2*$^{+/+}$*; Atoh1*$^{LacZ/flox}$; (C, E) *Egr2*$^{+/+}$*; Atoh1*$^{+/flox}$; (B, D, F) *Egr2; Atoh1*^{CKO}. (A, B) Wholemount β-galactosidase staining of P0 cochleae. The *Atoh1*^{LacZ} allele is expressed by hair cells in the cochlea and vestibular system. A continuous line of staining is seen in cochleae from both genotypes, suggesting that the majority of hair cells are present. (C, D) H&E-stained mid-modiolar sections of 6–7 week old cochlea. The overall structure appears normal in the *Egr2; Atoh1*^{CKO} animal. Asterisks mark the spiral ganglion. (E, F) High magnification view of boxed areas in panels (C) and (D). The organ of Corti appears normal, with one row of inner (asterisk) and three rows of outer (bracket) hair cells present in the *Egr2; Atoh1*^{CKO} animal.

AC – anterior crista, AN – auditory nerve, HC – horizontal crista, PC – posterior crista, Sac – saccule, ST – scala tympani, SV – scala vestibuli, Utr – utricle. Scale bars: (A, B) 1 mm, (C, D) 200 μm, (E, F) 10 μm.

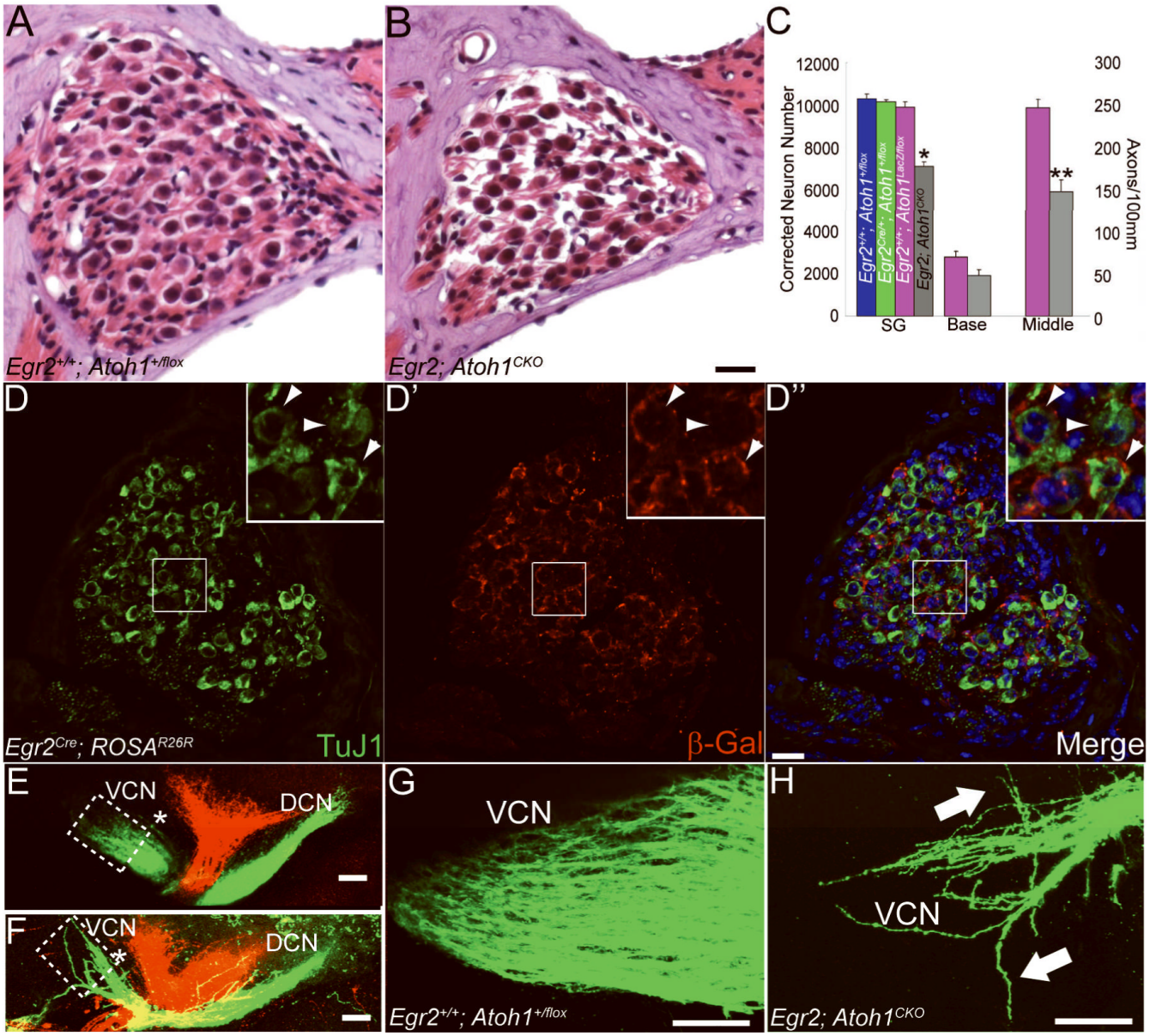

Figure 5.

SGN and auditory nerve axon number are decreased in *Egr2; Atoh1*^{CKO} animals, and auditory nerve axons show pathfinding errors in the CN. (A, B) Hematoxylin and eosin stained SG of 6 week old wildtype (A) and *Egr2; Atoh1*^{CKO} (B) animals. Note the decreased packing density in the *Egr2; Atoh1*^{CKO} SG. (C) Total SG neuron number and auditory nerve axon number at the base and middle of the cochlea. Error bars show SEM. All three populations are reduced by roughly 30% in *Egr2; Atoh1*^{CKO} animals relative to wildtype (T-test, *p = 0.01, **p = 0.004). (D–D″) SG sections from an adult *Egr2*^{Cre}*; ROSA*^{R26R} animal immunostained for TuJ1 and β-galactosidase. Insets show higher magnification views of the boxed region in each panel. Arrowheads denote TuJ1-positive neurons that are surrounded by *Egr2*-lineal cells. (EH) Lipophilic dye injections into the apex (green) and base (red) of P0 wildtype (E, G) and *Egr2; Atoh1*^{CKO} (F, H) cochlea label auditory nerve projections into the VCN and DCN. The VCN projections, particularly those from the apex of the cochlea, are much thinner in *Egr2; Atoh1*^{CKO} mice, and fibers aberrantly defasciculate and travel in abnormal anterior and

posterior directions (arrows in H). Boxes in (E) and (F) delineate areas shown in (G) and (H), respectively. * denotes the body of the VCN, which is much smaller in the *Egr2; Atoh1*^{CKO} CN. Projections to the DCN in *Egr2; Atoh1*^{CKO} animals are present and appear to be less affected than their VCN counterparts. Scale bars: (A, B, D–D″) 20 μm, (E–H) 100 μm.

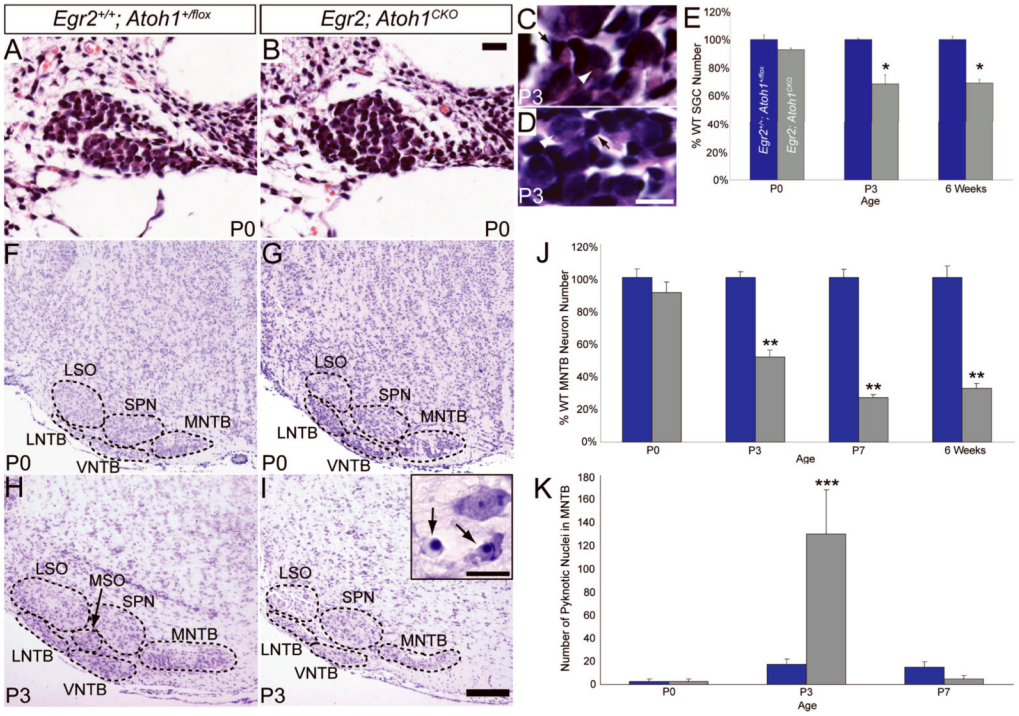

Figure 6.

Loss of neurons from the SG and AAN is a secondary effect of *Atoh1* disruption. (A, B) Hematoxylin and eosin-stained P0 wildtype (A) and *Egr2; Atoh1*^{CKO} (B) SGs. No cell loss is evident in the *Egr2; Atoh1*^{CKO} SG at this age. (C, D) Hematoxylin and eosin-stained P3 wildtype (C) and *Egr2; Atoh1*^{CKO} (D) SG. White arrowheads denote SGNs; black arrows denote glial cells. (E) *Egr2; Atoh1*^{CKO} SGN number graphed as a percentage of wildtype number at P0, P3 and 6 weeks of age. All of the cell loss in the SGN population occurs between P0 and P3 (T-test, *p = 0.02). (F–I) Cresyl violet stained coronal brainstem sections. (F, G) P0 AAN are identical in wildtype (F) and *Egr2; Atoh1*^{CKO} (G) brains. (H, I) Neuronal loss is present at P3 in the LNTB, MNTB and VNTB of *Egr2; Atoh1*^{CKO} mice (I). Inset in (I) shows pyknotic nuclei (arrows) in the MNTB. (J) *Egr2; Atoh1*^{CKO} MNTB neuron number graphed as a percentage of wildtype number at P0, P3, P7 and 6 weeks of age. The majority of the neuronal loss occurs between P0 and P3 (T-test, **p < 0.001). (K) Number of pyknotic nuclei in the MNTB at P0, P3 and P7. (T-test, ***p = 0.05). The time course of neuronal loss is the same in the SG and AAN. Scale bars: (A, B) 20 μm, (C, D, inset) 10 μm, (F–I) 200 μm.